Krzysztof WIERZCHOLSKI*

OPTIMUM NET FOR NUMERICAL REYNOLDS SOLUTIONS IN TRIBOLOGY

OPTYMALNE SIECI ROZWIĄZAŃ NUMERYCZNYCH REYNOLDSA W TRIBOLOGII

Słowa kluczowe:

Cząstkowe rekurencyjne równania Reynoldsa,optymalne rozwiązania numeryczne,współrzędne krzywoliniowe

Key words:

Partial recurrence Reynolds equations**,** optimum net for numerical solutions, curvilinear coordinates

Summary

The main scientific topic of the presented paper concerns the method of the determination of the optimum net for numerical solutions of partial recurrence Reynolds equations occurring in the hydrodynamic theory of lubrication. The abovementioned optimum of recurrence numerical calculation net refers to the stability of particular and general numerical solutions of partial recurrence modified Reynolds equations in curvilinear coordinates.

* Koszalin University of Technology,Institute of Technology and Education, PL 75-453, Koszalin, Śniadeckich 2, Poland; ; krzysztof.wierzcholski@wp.pl.

INTRODUCTION

From the mathematical point, the presented method of the solution of the modified Reynolds equation occurring in tribology leads to the problem of resolving the partial recurrence non-homogeneous equation of the second order with variable coefficients [**L. 1–4**]. Furthermore, taking into account the UOS method [**L. 5**], the topology of solutions presented in this paper on the space of the discrete values for partial recurrence equations makes it possible to select optimum numerical methods [**L.6–10**]. Hence, this paper considers an optimum scheme of recurrent performances and an optimum net for recurrent calculations from among many methods in relation to the stability of solutions, and the convergence of obtained calculations occurring in the hydrodynamic theory of lubrication [**L. 8**].

In this paper, we will assume an optimum difference scheme which leads from the recurrent partial equation with known Dirichlet boundary conditions as a model to recurrent Reynolds equations as an application in tribology. To the author's knowledge, such problems have not been considered in scientific researches in the field of the numerical methods of hydrodynamic theory of classical slide-bearing lubrication as well as in analytical and numerical theory of microbearing lubrication occurring in computer HDD [**L. 11–20**].

We consider the orthogonal, curvilinear coordinates (α_1, α_2, α_3). Let function P(x,z) of two variables α_1= x, α_3= z be determined on region A×A:Ω:{(x,z) for 0≤x,z≤A}. The region is covered over the net created by the straight lines parallel to the axis α_1=x, α_3=z in the sub-intervals by distance h and k respectively. Such a division can be defined in the following form [**L. 2**, **19**, **20**]:

$$\begin{aligned} &h \equiv \alpha_{1i+1} - \alpha_{1i}, \quad k \equiv \alpha_{3j+1} - \alpha_{3j}, \\ &i = 1,2,...,M;\ j = 1,2,...,N \end{aligned} \tag{1}$$

The cut points of the above-mentioned lines form the nod inside region A×A are presented in **Fig. 1.**

Now we describe numerical hydrodynamic pressure distribution between two surfaces in orthogonal curvilinear coordinates *(α_1,α_2,α_3)*. The Reynolds equation for unknown pressure function p(α_1,α_3) is formulated in the following form **[L. 6]**:

$$\begin{aligned} &C(\alpha_1,\alpha_3)\frac{\partial}{\partial\alpha_1}\left[A(\alpha_1,\alpha_3)\frac{\partial p}{\partial\alpha_1}\right] + F(\alpha_1,\alpha_3)\frac{\partial}{\partial\alpha_3}\left[B(\alpha_1,\alpha_3)\frac{\partial p}{\partial\alpha_3}\right] = \\ &= G(\alpha_1,\alpha_3)\frac{\partial H(\alpha_1,\alpha_3)}{\partial\alpha_1} \end{aligned} \tag{2a}$$

a)

b)

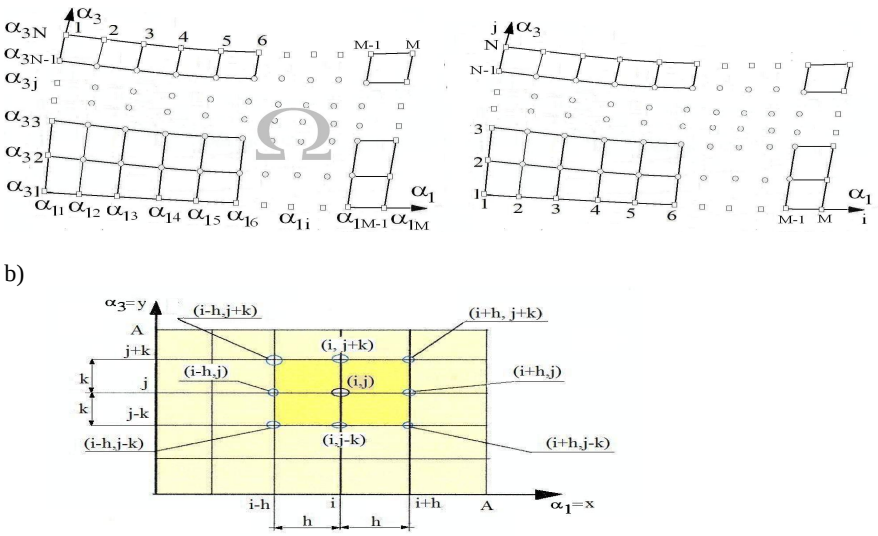

Fig. 1. Curvilinear orthogonal coordinate system: a) region Ω, b) calculation nod
Rys. 1. Układ współrzędnych krzywoliniowych: a) obszar Ω, b) węzeł obliczeniowy

where $p(\alpha_1,\alpha_3)=\Phi(\alpha_1,\alpha_3)$, $(\alpha_1,\alpha_3)\in\partial\Omega$. After terms ordering we have **[L.6]**:

$$C\frac{\partial A}{\partial\alpha_1}\frac{\partial p}{\partial\alpha_1}+CA\frac{\partial^2 p}{\partial\alpha_1^2}+F\frac{\partial B}{\partial\alpha_3}\frac{\partial p}{\partial\alpha_3}+FB\frac{\partial^2 p}{\partial\alpha_3^2}=G\frac{\partial H}{\partial\alpha_1} \tag{2b}$$

We denote

$$A(\alpha_1,\alpha_3)\equiv\int_0^{\varepsilon}\left[\int_0^{\alpha_2}\frac{\alpha_2 d\alpha_2}{\eta(\alpha_1,\alpha_2,\alpha_3)}-\frac{\int_0^{\alpha_2}\frac{d\alpha_2}{\eta(\alpha_1,\alpha_2,\alpha_3)}}{\int_0^{\varepsilon}\frac{d\alpha_2}{\eta(\alpha_1,\alpha_2,\alpha_3)}}\int_0^{\varepsilon}\frac{\alpha_2 d\alpha_2}{\eta(\alpha_1,\alpha_2,\alpha_3)}\right]d\alpha_2 \tag{3a}$$

$$B(\alpha_1,\alpha_3)\equiv\frac{h_1(\alpha_1,\alpha_3)}{h_3(\alpha_1,\alpha_3)}A(\alpha_1,\alpha_3),\ C(\alpha_1,\alpha_3)\equiv\frac{1}{h_1(\alpha_1,\alpha_3)} \tag{3b}$$

$$F(\alpha_1,\alpha_3)\equiv\frac{1}{h_3(\alpha_1,\alpha_3)},\quad G(\alpha_1,\alpha_3)\equiv\omega\, h_1(\alpha_1,\alpha_3) \tag{3c}$$

$$H(\alpha_1,\alpha_3) \equiv \int_0^{\varepsilon} \left(\frac{\int_0^{\alpha_2} \frac{d\alpha_2}{\eta(\alpha_1,\alpha_2,\alpha_3)}}{\int_0^{\varepsilon} \frac{d\alpha_2}{\eta(\alpha_1,\alpha_2,\alpha_3)}} \right) d\alpha_2 - \varepsilon(\alpha_1,\alpha_3) \tag{3d}$$

whereas

$\varepsilon(\alpha_1,\alpha_3)$ – various gap height between two cooperating surfaces,
$h_s(\alpha_1,\alpha_3)$ – Lame functions for $s=1,3$ depend on the kind of surface,
ω – angular velocity of in the case of rotational surface,
$\eta(\alpha_1,\alpha_2,\alpha_3)$ – dynamic fluid viscosity.

THE RECURRENT TAYLOR MODEL

The Taylor series are important for the application for the transformation to the recurrence form [**L.6**]. Function P(x,z) of two variables is expanded in the Taylor series in the neighbourhood (h.k) of point (x+h,z+k):

$$P(x+h,z+k) = P(x,z) + \left(h\frac{\partial}{\partial x} + k\frac{\partial}{\partial z} \right) P(x,z) + \frac{1}{2!}\left(h\frac{\partial}{\partial x} + k\frac{\partial}{\partial z} \right)^2 P(x,z) + \ldots + \frac{1}{n!}\left(h\frac{\partial}{\partial x} + k\frac{\partial}{\partial z} \right)^n P(x+\Theta_x h, z+\Theta_z k) \tag{4}$$

where $0<\Theta_x,\Theta_z<1$.We assume the following notation of the derived functions:

$$\frac{\partial P}{\partial x} \equiv P_x, \quad \frac{\partial P}{\partial z} \equiv P_z, \quad \frac{\partial^2 P}{\partial x^2} \equiv P_{xx}, \quad \frac{\partial^2 P}{\partial z^2} \equiv P_{zz}, \quad \frac{\partial^2 P}{\partial x \partial z} \equiv P_{xz}, \ldots\ldots \tag{5}$$

Making use of Taylor formula (4) and taking into account notations (5), we lead function $P(x,z)$ in neighbourhood (i,j) into the following difference form:

$$P_{i+h,j+k} = P_{ij} + h(P_x)_{ij} + k(P_z)_{ij} + 0{,}5\, h^2(P_{xx})_{ij} + hk(P_{xz})_{ij} + 0{,}5\, k^2(P_{zz})_{ij} + O(h^3,k^3) \tag{6}$$

After ordering, we can write Equation (6) in the following difference form [**L. 2**].

$$0.5\,\{h^2 p_{xx} + k^2 p_{zz}\}_{ij} = p_{i+h,j+k} - p_{ij} - h(p_x)_{ij} - k(p_z)_{ij} - hk(p_{xz})_{ij} + O(h^3) + O(k^3) \tag{7}$$

FIRST AND SECOND MODEL OF UNIT NET REGION

Into Eq. (7) we put the two sets of the following four ordered pair values h, k [**L. 2**, **17**].

$$(h=1, k=0), (h=-1, k=0), (h=0, k=+1), (h=0, k=-1) \tag{8}$$

$$(h=-1, k=-1), (h=1, k=-1), (h=-1, k=+1), (h=1, k=+1) \tag{9}$$

From each of the two-abovementioned sets of four pair values (8) and (9) substituted into Eq. (7) gives another form of equations. We add these four obtained equations mutually. Thus, for (8), (9), we obtain the following recurrence UNR (Unit Net Region) forms [**L. 2**, **21**]:

$$\Delta_1 P_{ij} \equiv h^2 (P_{xx}+P_{zz})_{ij} = P_{i+1,j} + P_{i-1,j} + P_{i,j+1} + P_{i,j-1} - 4P_{i,j} + O_1(1) \tag{10}$$

for $O_1(1) \equiv -\Theta (P_{xxxx}+P_{zzzz})_{ij}$

$$\Delta_2 P_{ij} \equiv 2h^2 (P_{xx}+P_{zz})_{ij} = P_{i-1,j-1} + P_{i+1,j-1} + P_{i+1,j+1} + P_{i-1,j+1} - 4P_{i,j} + O_2 \tag{11}$$

for $O_2 = 2O_1 - (P_{xxzz})_{ij}$

where $\Theta = 1/12$. Dimension conformability demands to multiply the l.h.s. of Eqs. (10-11) by h^2 for h=k. **Figs. 2a, b** present the UNR net of nods for the difference form (10) and (11). For respective nods, the following coefficient values are ascribed: *1,1,1,1,–4* and *1,1,1,1,–4*. Such coefficients occur by the appropriately indicated terms of recurrent formulas (10) and (11), respectively [**L. 2**, **7**].

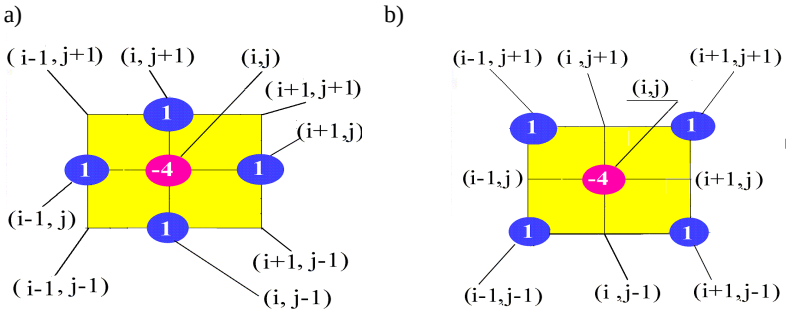

Fig. 2. The net with nods for a) first and b) second case of approximation difference form for UNRΔ_1 and Δ_2

Rys. 2. Siatka węzła numerycznego dla a) pierwszego oraz b) drugiego przypadku aproksymacji różnicowej UNRΔ_1 i Δ_2

In the net presented in **Fig. 2**, the internal nod is fourfold and the external nods are single. The fourfold nod denotes that, at the term $P_{i,j}$ in recurrent Eqs. (10), (11) coefficient 4 occurs. The external nods and the internal nod form the geometry element of the UNR [**L. 2**, **7**].

THIRD AND FOURTH MODEL OF UNIT NET REGION

The third case of the approximation difference form for UNR will be defined by the union of two foregoing forms and is described by the following formula [**L.2**, **7**, **21**].

$$\Delta_3 P_{ij} \equiv (a\,\Delta_1 + b\,\Delta_2)\,P_{ij} \quad \text{for } a = 1 \text{ and } b = 1 \tag{12}$$

Putting approximation forms (10)+(11) into (12), we obtain

$$\Delta_3 P_{ij} \equiv 3h^2(P_{xx}+P_{zz})_{ij} = P_{i-1,\,j-1} + P_{i,\,j-1} + P_{i+1,\,j-1} + P_{i-1,\,j} +$$

$$+ P_{i+1,\,j} + P_{i+1,j+1} + P_{i-1,\,j+1} + P_{i,\,j+1} - 8P_{i,j} + O_3 \quad \text{for} \quad O_3 \equiv O_1 + O_2 \tag{13}$$

Fig. 3a presents the net of nods for difference form (13). To respective nods, the following coefficient values are ascribed: *1,1,1,1,1,1,1,1,–8* occurring by the appropriately indicated terms of recurrent formula (13).

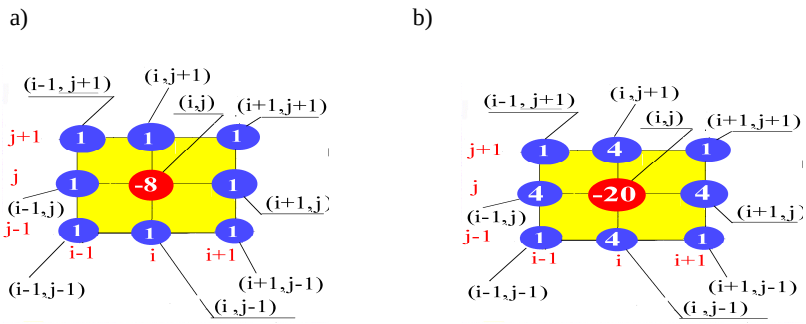

Fig. 3. The net with nods for a) third and b) fourth case of approximation difference form for UNR Δ_3 and Δ_4

Rys. 3. Siatka węzła numerycznego dla a)trzeciego oraz b)czwartego przypadku aproksymacji różnicowej UNR Δ_3 i Δ_4

In the presented net in Fig.3a, the internal nod is eightfold and the external nods are single. The eightfold nod denotes that, in recurrent equations (13) at term $P_{i,j}$ the coefficient 8 occurs. The external nods and the internal nod form the element of the UNR.

The fourth case of the approximation difference form for UNR will be defined by the combination of two foregoing forms using the following formula [**L. 2**, **7**, **21**].

$$\Delta_4 P_{ij} \equiv (a\,\Delta_1 + b\,\Delta_2)\,P_{ij} \quad \text{for } a = 4 \text{ for } b = 1 \tag{14}$$

We put approximation forms (10)+(11) in Eq. (14). Thus, we obtain

$$\Delta_4 P_{ij} \equiv 6h^2 (P_{xx} + P_{zz})_{ij} = 4(P_{i-1,j} + P_{i+1,j} + P_{i,j-1} + P_{i,j+1} + P_{i-1,j-1} +$$

$$+ P_{i+1,j-1} + P_{i+1,j+1} + P_{i-1,j+1} - 20P_{ij} + O_4, \qquad \text{for } O_4 \equiv 4O_1 + O_2 \tag{15}$$

Fig. 3b presents the net of nods for difference form (14).

For respective nods, the following coefficient values are ascribed: *1,4,1,4,1,4,1,4,–20* occurring by the appropriately indicated terms of recurrent formula (15). In the net presented in **Fig. 4**, the internal centre nod is twenty fold and the four corner external nods are single; whereas, the remaining external nods are fourfold. The twenty fold centre nod denotes that, at term $P_{i,j}$ coefficient 20 occurs in recurrent equations (14). The external nods and the internal nod form the element of the UNR.

INDEX FOR NET OPTIMIZATION

Now we show the way of the stability evaluation of numerical solutions for the individual difference approximations of UNR. We define the following optimization index:

$$c \equiv \frac{\Pi}{\sum_{r=1}^{R} W_r} \tag{16}$$

where r – the index of movable nod in the element of net ($r = 1,2,..,R$), R – the quantity of possible movable nods in an element of the net, W_r – the multiplicity of coefficients in the r-th movable nod during the conversion step from one to the next position in the numerical calculations of the recurrence equation, Π **–** the multiplicity of covering of non-zero coefficients in all the nods during the conversion step from one position to the next position in the numerical calculations of the recurrence equation. Index c denotes the ratio of the cover quantity of non-zero coefficients to the one movable coefficient during the conversion from one position to the next position of the net element in the numerical calculations. The stability of the calculation process increases if index c increases.

OPTIMIZATION INDEX FOR NET CONVERSION

Now we calculate optimization index c for the above-mentioned recurrence UNR forms of approximation.

- **Fig. 4** illustrates the conversion of the net element with movable nods from one position to the next position during the numerical process in the first case of the approximation difference form i.e. for UNR Δ_1.

  In the mentioned case, we have R = 5, $\Pi = 1 + 1 = 2$, and

$$\Sigma W_r = 1 + 1 + 4 + 1 + 1 = 8 \quad \text{and} \quad c = 2/8 = 0.25. \tag{17}$$

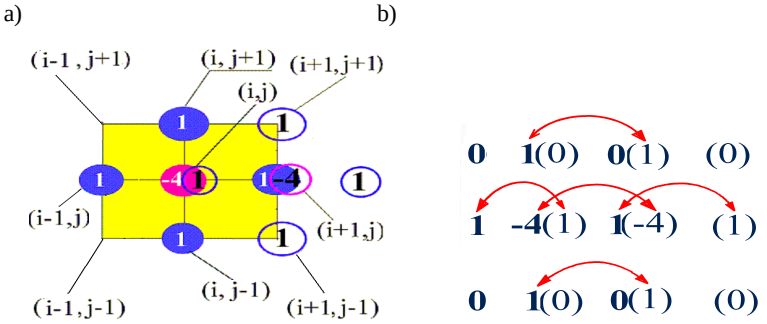

Fig. 4. The covering geometry of nods during the conversion of the movable net element from one to the next position in numerical calculations for the first UNR Δ_1 approximation form: a) origin nods geometry , b) movement of the elements

Rys. 4. Geometria pokrycia topologicznego węzła podczas konwersji ruchomej siatki z jednej do drugiej pozycji w obliczeniach numerycznych pierwszej aproksymacji UNR Δ_1, a) geometria węzła,b) ruch elementu

- **Fig.5** illustrates the conversion of the net element with movable nods from one position to the next position during the numerical process in the second case of the approximation recurrence form for UNR Δ_2.

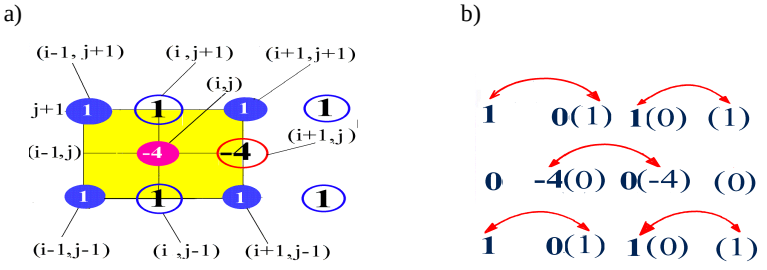

Fig. 5. The covering geometry of nods during the conversion of the movable net element from one to the next position in numerical calculations for second UNR Δ_2 approximation form: a) origin nods geometry , b) movement of the elements

Rys. 5. Geometria pokrycia topologicznego węzła podczas konwersji ruchomej siatki z jednej do drugiej pozycji siatki w obliczeniach numerycznych drugiej aproksymacji UNR Δ_2, a) geometria węzła,b) ruch elementu

In the above-mentioned case, we have R = 5, Π = 0, and

$$\Sigma W_r = 1+1+4+1+1 = 8 \text{ and } c = 0/8 = 0 \tag{18}$$

- **Fig.6** illustrates the conversion of the net element with movable nods from one position to the next position during the numerical process in the third case of the approximation recurrence form for UNR Δ_3.

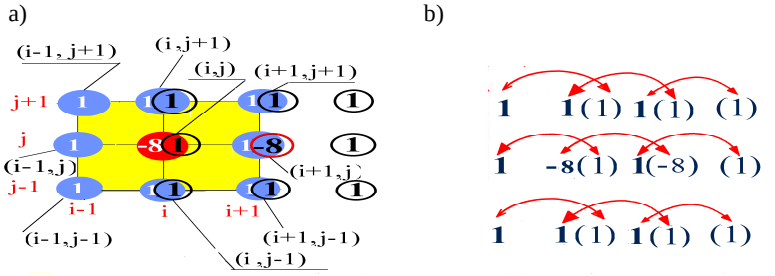

Fig. 6. The covering geometry of nods during the conversion of the movable net element from one to the next position in numerical calculations for third UNR Δ_3 approximation form: a) origin nods geometry , b) movement of the elements

Rys. 6. Geometria pokrycia topologicznego węzła podczas konwersji ruchomej siatki z jednej do drugiej pozycji siatki w obliczeniach numerycznych trzeciej aproksymacji UNR Δ_2, a) geometria węzła,b) ruch elementu

In the above-mentioned case, we have: R=9, Π=6×1=6,

$$\Sigma W_r = 1+1+1+1+1+8+1+1+1+1 = 16 \tag{19}$$

and optimization index equals c=6/16=**0.375.**

- **Fig. 7** illustrates the conversion of the net element with movable nods from one position to the next position during the numerical process in the fourth case of the approximation recurrence form for UNR Δ_4 [**L. 2**, **7**, **22**].

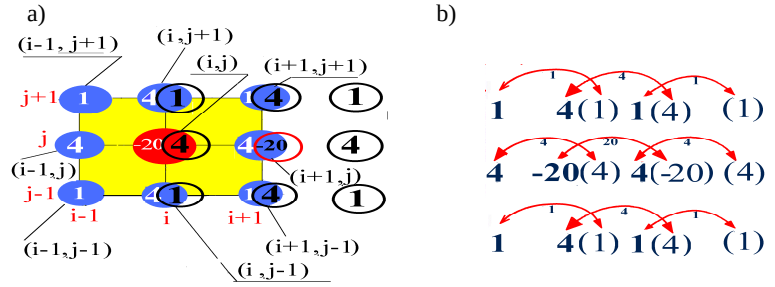

Fig. 7. The covering geometry of nods during the conversion of the movable net element from one to the next position in numerical calculations for four UNR Δ_4 approximation form: a) origin nods geometry, b) movement of the elements

Rys. 7. Geometria pokrycia topologicznego węzła podczas konwersji ruchomej siatki z jednej do drugiej pozycji siatki w obliczeniach numerycznych czwartej aproksymacji UNR Δ_2, a) geometria węzła, b) ruch elementu

In mentioned case, we have R=9, $\mathbf{\Pi}$=1+1+4+4+1+1=12,

$$\Sigma W_r=1+4+1+4+20+4+1+4+1=40,\ c=12/40=0.300 \tag{20}$$

- COROLLARY. *In the succeeding cases presented for numerical procedures, we have the following values of optimization coefficients: 0.25, 0.00, 0.375, and 0.300. In numerical calculations, the third case is the most stable, because optimization index c is the largest and has value 0.375.*

REYNOLDS RECURRENCES FOR FIRST UNR MODEL

For first UNR step where nods are presented in Fig. 2a, we seek the unknown pressure solution *p* from equation (2b), taking into account progressive differences in the difference method and recurrence equations in lubrication region domain $\Omega(\alpha_1,\alpha_3)$. This curvilinear region $\boldsymbol{\Omega}$ indicated in Fig.1a contains *NM* nods, where there are *2M+2N–4* varies nods on the boundary of the region and NM–2(N+M)+4 internal nods. The values of the functions *A, B, C,F, G,* in the nods $w_{ij}=(\alpha_1=\alpha_{1i},\ \alpha_3=\alpha_{3j})$ of divided region $\boldsymbol{\Omega}$ for *i=1,2,…,M–1,M; j=1,2,…,N–1,N* we denote by the following formulae [**L.4**].

$$\begin{aligned} &A(w_{ij})\equiv A_{i,j},\quad B(w_{ij})\equiv B_{i,j},C(w_{ij})\equiv C_{i,j},F(w_{ij})\equiv F_{i,j},G(w_{ij})\equiv G_{i,j},\\ &p(\alpha_1=\alpha_{1i},\alpha_3=\alpha_{3j})=p(w_{ij})\equiv p_{i,j} \end{aligned} \tag{21}$$

Taking into account steps of division (1) and progressive differences, then we obtain [**L.7**] the following:

$$\left(\frac{\partial A}{\partial\alpha_1}\right)_i\left(\frac{\partial p}{\partial\alpha_1}\right)_i\approx p_{i+1,j}\frac{A_{i+1,j}-A_{i,j}}{h^2}-p_{i,j}\frac{A_{i+1,j}-A_{i,j}}{h^2} \tag{22}$$

$$\left(\frac{\partial B}{\partial\alpha_3}\right)_j\left(\frac{\partial p}{\partial\alpha_3}\right)_j\approx p_{i,j+1}\frac{B_{i,j+1}-B_{i,j}}{k^2}-p_{i,j}\frac{B_{i,j+1}-B_{i,j}}{k^2} \tag{23}$$

The pressure function *p(x,z)* for $\alpha_1\equiv x$, $\alpha_3\equiv z$ is expanded in the Taylor series in the neighbourhood of the point *(x+h,z+k)* in form (4). Taking into account the index differentiation (5) of the function *p(x,z)* in the neighbourhood of the point *(i,j),* the Taylor formula (4) tends to the dependence (6) and finally to expression (7). Accordingly to the assumption (8), we put *h=1, k=0* and *h= –1, k=0* into formula (7); thus, we obtain two equations, respectively. Next, we multiply both sides of the obtained equations by *CA*. If we sum up the obtained equations, after division by h^2, we obtain the following:

$$CA\frac{\partial^2 p}{\partial \alpha_1^2} = \frac{C_{i,j}A_{i,j}}{h^2}p_{i+1,j} + \frac{C_{i,j}A_{i,j}}{h^2}p_{i-1,j} - 2\frac{C_{i,j}A_{i,j}}{h^2}p_{i,j}, \alpha_1 \equiv x \tag{24}$$

Accordingly to the assumption (8), we put h=0, k=1 and h=0, k=−1 into formula (7); thus, we obtain two equations, respectively. Next, we multiply both sides of the obtained equations by FB. If we sum up the obtained equations, after division by k^2, we obtain the following [**L.7**]:

$$FB\frac{\partial^2 p}{\partial \alpha_3^2} = \frac{F_{i,j}B_{i,j}}{k^2}p_{i,j+1} + \frac{F_{i,j}B_{i,j}}{k^2}p_{i,j-1} - 2\frac{F_{i,j}B_{i,j}}{k^2}p_{i,j}, \alpha_3 \equiv z \tag{25}$$

If we put dependencies (22),(23),(24), and (25) into partial differential equation (2b), and taking into account formulas (21), then for each nod from **Fig.2a**, we obtain the following partial recurrence equations of the second order with variable coefficients, for the first UNR step [**L.7**]:

$$\kappa_{i+1,j}p_{i+1,j} + \nu_{i,j+1}p_{i,j+1} + \pi_{i,j-1}p_{i,j-1} + \xi_{i-1,j}p_{i-1,j} - Z_{i,j}p_{i,j} = Q_{i,j} \tag{26}$$

where for *i=1,2,…,M–1,M; j=1,2,…,N–1,N*, we have the following coefficients [**L.4**]:

$$\kappa_{i+1,j} \equiv \frac{C_{i,j}A_{i+1,j}}{h^2}, \quad \nu_{i,j+1} \equiv \frac{F_{i,j}B_{i,j+1}}{k^2}, \xi_{i-1,j} \equiv \frac{C_{i,j}A_{i,j}}{h^2}, \pi_{i,j-1} \equiv \frac{F_{i,j}B_{i,j}}{k^2} \tag{27}$$

and

$$Z_{i,j} \equiv \kappa_{i+1,j} + \nu_{i,j+1} + \pi_{i,j-1} + \xi_{i-1,j}, Q_{i,j} \equiv G_{i,j}\frac{H_{i+1,j} - H_{i,j}}{h} \tag{28}$$

REMARK 1. *Similar to the net presented in Fig.2a, the internal nod coefficient Z in Eq. (28) denotes the sum of external coefficients described in Eqs. (27).*

If we translate one step of index i and j in both sides of Eq. (26), we obtain a partial recurrence equation of the second order with variable coefficients in the standard form. The sequence of pressure values $\{p_{i,j}\}$ with unknown elements presenting the pressure values in nods of the region Ω is the solution of the partial recurrence equation (26); however, the coefficients (27) and free term $Q_{i,j}$ are known. If we take the same number of steps in α_1 and α_3 directions, i.e. *M=N*, then the region $\Omega(\alpha_1,\alpha_3)$ presented in **Fig. 1a** has $(N–2)^2$ internal nods *(i,j)* illustrated in **Fig. 2a** for *i=2,…,N–1; j=2,…,N–1*. If we put index values *i* and *j* for the each internal nod into equation (26), then we obtain

an algebraic system of $(N–2)^2$ linear, non-homogeneous equations with $(N–2)^2$ unknown. We assume known values Φ in $4N–4$ external nods of the region $\Omega(\alpha_1,\alpha_3)$ in the form of the following boundary conditions:

$$p_{k,j}= \Phi_{k,j},\ p_{i,k}= \Phi_{i,k},\ \text{for } k=1,N\ ;\ i,j=1,\ldots,N–1,N;\ \Phi_{i,j}=\Phi(\alpha_i,\ \alpha_j) \tag{29}$$

REYNOLDS RECURRENCES FOR THIRD UNR MODEL

For third Unit Net Region (UNR) step, where nods are presented in **Fig. 3**, we seek the unknown pressure solution p from Equation (3b), taking into account the difference method and recurrence equations in lubrication region domain $\Omega(\alpha_1,\alpha_3)$. Accordingly to the assumption (9), we put $(h = –1, k = –1), (h = 1, k = –1), (h = –1,k = +1), (h = 1,k = +1)$ into formula (7); thus, we obtain the four equations, respectively. We mutually add the obtained equations; hence, we obtain [**L.2**, **7**, **22**] as follows:

$$2(h^2 p_{xx} + k^2 p_{zz}) = p_{i-1,j-1} + p_{i+1,j-1} + p_{i-1,j+1} + p_{i+1,j+1} - 4p_{i,j} \tag{30}$$

From Eq. (30) for k=0 and for h=0, we obtain two expressions which we multiply by CA and FB and divide by h^2 and k^2, respectively. After ordering terms we obtain the following:

$$CA\frac{\partial^2 p}{\partial x^2} = \frac{C_{i,j}A_{i,j}}{2h^2}\left(p_{i-1,j-1} + p_{i+1,j-1} + p_{i-1,j+1} + p_{i+1,j+1}\right) - 2\frac{C_{i,j}A_{i,j}}{2h^2}p_{i,j} \tag{31}$$

$$FB\frac{\partial^2 p}{\partial z^2} = \frac{F_{i,j}B_{i,j}}{2k^2}\left(p_{i-1,j-1} + p_{i+1,j-1} + p_{i-1,j+1} + p_{i+1,j+1}\right) - 2\frac{F_{i,j}B_{i,j}}{k^2}p_{i,j} \tag{32}$$

Equations (22), (23), (30), and (31) we put into differential Eq. (3b). With the obtained equation, we mutually sum with equation (26). After ordering terms for each nod from Fig. 3, we obtain the following partial recurrence equations of the second order with variable coefficients for the third UNR step:

$$\begin{aligned}&\beta_{i,j}\left(p_{i-1,j-1} + p_{i+1,j-1} + p_{i-1,j+1} + p_{i+1,j+1}\right) + \delta_{i+1,j}p_{i+1,j} + \chi_{i,j+1}p_{i,j+1} + \\ &+\pi_{i,j-1}p_{i,j-1} + \xi_{i-1,j}p_{i-1,j} - Y_{i,j}p_{i,j} = 2Q_{i,j}\end{aligned} \tag{33}$$

where

$$\beta_{i,j} \equiv 0{,}5(\xi_{i-1,j} + \pi_{i,j-1}),\ \delta_{i+1,j} \equiv 2\kappa_{i+1,j} - \xi_{i-1,j},\ \chi_{i,j+1} \equiv 2\nu_{i,j+1} - \pi_{i,j-1} \tag{34}$$

$$Y_{i,j} \equiv 2Z_{ij} = 2\left(\kappa_{i+1,j} + \nu_{i,j+1} + \pi_{i,j-1} + \xi_{i-1,j}\right), Q_{i,j} \equiv G_{i,j}\frac{H_{i+1,j} - H_{i,j}}{h} \tag{35}$$

After the foregoing considerations, we confirm that the abovementioned third UNR step approximation is the best, because, in this case, the optimization index is greatest. This case determines the optimum net for the recurrence Reynolds equation.

REMARK 2. *Similar to the net presented in Fig.3a, the internal nod coefficient Y in Eq.(33) denotes the sum of external coefficients described in Eqs. (34).*

To prove the above statement we have the following:

$$\begin{aligned}&\delta_{i+1,j} + \chi_{i,j+1} + \pi_{i,j-1} + \xi_{i-1,j} + 4\beta_{i,j} = 2\kappa_{i+1,j} + 2\nu_{i,j+1} + 2\pi_{i,j-1} + 2\xi_{i-1,j} = \\ &= 2Z_{i,j} = Y_{i,j}\end{aligned} \tag{36}$$

NUMERICAL COMPARISON FOR PRESSURE AND CAPACITY IN THE FIRST AND THIRD UNR APPROXIMATION

■ **Cylindrical slide journal bearing.** In this intersection, the hydrodynamic pressure is numerically examined for a microbearing with a cylindrical journal by virtue of partial recurrence Equation (26) in the first UNR step, and the obtained results are compared with the pressure values obtained from recurrence Equation (36) in the third UNR step. Both recurrence equations (26) and (36) are simulated from Reynolds equations (2a), (2b) for continuous functions.

We consider the cylindrical microbearing in cylindrical coordinates $\alpha_1 = \varphi, \alpha_2 = r, \alpha_3 = z$, for journal radius $R = 0.001$ [m], bearing dimensionless length $L_{cy} = b_{cy}/R = 1$, b_{cy}–dimensional bearing length angular journal velocity $\omega = 565.5$[1/s], and eccentricity ratio $\lambda_{cy} = 0.4$. We assume a constant value of oil dynamic viscosity $\eta = \eta_0 = 0.03$ [Pas], and obtain an angular coordinate of film end attains value $\varphi_k = 3.658$ [rad]. For a thin layer, the Lame coefficients and gap height have the following values **[L. 6]**:

$$h_1 = h_\varphi = R,\ h_3 = h_z = 1 \tag{37}$$

$$\varepsilon(\varphi) = \varepsilon_0(1 + \lambda_{cy}\cos\varphi) \tag{38}$$

Because characteristic pressure is assumed $p_0 = 16.96$ [MPa], the radial clearance has the value the following [**L. 23**]:

$$\varepsilon_0 = R\sqrt{\frac{\omega\eta_0}{p_0}} = 0,001m\sqrt{\frac{565.5s^{-1}0,03Pas}{16,96MPa}} \approx 1,3\mu m. \tag{39}$$

Numerical dimensional pressure values as the solutions of partial recurrence Equation (26) for first UNR step performed with the Mathcad 12 and Matlab 7.2 Professional Program are depicted on the cylindrical journal surface presented in **Fig. 8a**. The hydrodynamic pressure attains maximum value p_{max} = 21.73 [MPa] and load carrying capacity C_{tot} = 40.46N.

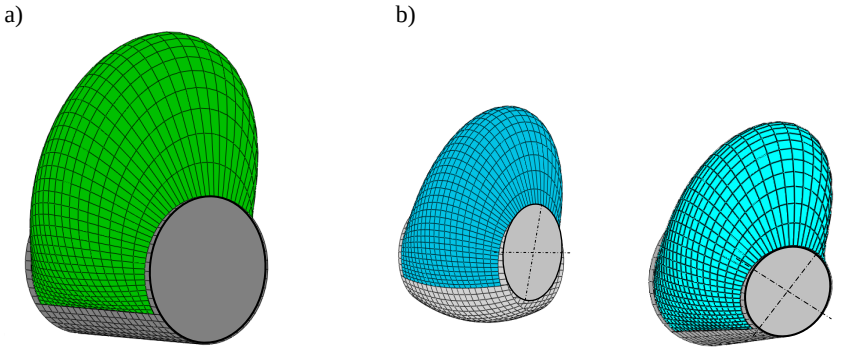

Fig. 8. Dimensional hydrodynamic pressure distribution in microbearing gap obtained from recurrence equation (26) in first UNR step for various journal shapes: a) cylindrical , b) parabolic, c) conical

Rys. 8. Wymiarowe ciśnienie hydrodynamiczne w szczelinie cylindrycznego mikrołożyska wyznaczone numerycznie z równania (26) w pierwszym kroku UNR dla różnych kształtów czopów: a) walcowych, b) parabolicznych, c) stożkowych

For the abovementioned cylindrical microbearing, differences between pressure values obtained from recurrence Reynolds Equation (26) derived for the first UNR classical net and pressure values obtained from Equation (33) derived for the third UNR optimum net approximation, attain about 9 percent.

■ **Parabolic slide-journal bearing.** In this intersection, the hydrodynamic pressure is numerically examined for microbearings with a parabolic journal and sleeve by virtue of partial recurrence Equation (26) in the first UNR step, and the next obtained results are compared with the pressure values obtained from recurrence Equation (36) in third UNR step. Both recurrence equations (26) and (36) are simulated from Reynolds Equations (2a), (2b) for continuous functions. We consider parabolic microbearing in parabolic coordinates $\alpha_1 = \varphi$, $\alpha_2 = y_p$, $\alpha_3 = \xi_p$, for journal largest radius $a = 0.001$ [m], the journal's smallest radius $a_1 = 0.0008$ [m] bearing dimensionless length $L_{p1}=b_p/a=1$, b_p–dimensional bearing length, angular journal velocity $\omega=741$[1/s], eccentricity ratio $\lambda_p = 0.5$. We assume a constant

value of oil dynamic viscosity $\eta=\eta_0=0.030$ [Pas], and obtain an angular coordinate of film end having a value of $\varphi_k=3.665$ [rad]. For a thin layer, the Lame coefficients and gap height have the following form [**L. 6, 23**]:

$$h_1 = a\cos^2\left(\Lambda_{p1}\zeta_{p1}\right), \quad h_3 = \sqrt{1+4\left(\Lambda_{p1}/L_{p1}\right)^2 \sin^2\left(\Lambda_{p1}\zeta_{p1}\right)}\cos\left(\Lambda_{p1}\zeta_{p1}\right)$$
$$\left|\zeta_{p1}\right| \le \frac{1}{\Lambda_{p1}}\arccos\sqrt{\frac{a_1}{a}},\ \Lambda_{p1} \equiv \sqrt{\frac{a-a_1}{a}}, \zeta_{p1} = \frac{\zeta_p}{b_p} \tag{40}$$

$$\varepsilon(\varphi) = \varepsilon_0(1 + \lambda_p\cos\varphi) \tag{41}$$

Because characteristic pressure is assumed $p_0 = 5.655$ *[MPa]*, the radial clearance has the following value:

$$\varepsilon_0 = a\sqrt{\frac{\omega\eta_0}{p_0}} = 0,001\,m\sqrt{\frac{741s^{-1}0,03Pas}{5,655MPa}} \approx 2,6\,\mu m \tag{42}$$

Numerical dimensional pressure values as the solutions of partial recurrence Equation (26) for first UNR step performed with the Mathcad 12 and Matlab 7.2 Professional Program are depicted on the parabolic journal surface presented in **Fig. 8b.** The hydrodynamic dimensional pressure attains a maximum value of p_{max} = 11.98 [MPa] and load carrying capacity C_y=20.16N.

For the abovementioned parabolic microbearing, the differences between pressure values obtained from recurrence Reynolds Equation (26) derived for the first UNR classical net and pressure values obtained from Equation (33) derived for the third UNR optimum net approximation, attain about 10 percent.

■ **Conical slide-journal bearing.** In this section, the hydrodynamic pressure is numerically examined for microbearing with a conical journal and sleeve by virtue of partial recurrence Equation (26) in first UNR step, and the obtained results are compared with the pressure values obtained from recurrence Equation (36) in the third UNR step. Both recurrence equations (26) and (36) are simulated from Reynolds Equation (2a), (2b) for continuous functions. We consider parabolic microbearings in parabolic coordinates $\alpha_1 = \varphi, \alpha_2 = y_c$, $\alpha_3 = x_c$, for journal radius $R = 0.001$ [m], conical inclination angle $\gamma = 70^0$, bearing dimensionless length $L_{c1} = b_c/R = 1$, b_c – dimensional bearing length, angular journal velocity $\omega = 754[1/s]$, and eccentricity ratio $\lambda_c = 0.5$.

We assume a constant value of oil dynamic viscosity $\eta = \eta_0 = 0.025$ [Pas], and obtain an angular coordinate of film end having a value of $\varphi_k = 3.600$ [rad]. The Lame coefficients and gap height have the following form [**L. 6**, **7**, **23**]:

$$h_1 = h_\varphi = R + x_c \cos\gamma,\ h_3 = h_y = 1 \tag{43}$$

$$\varepsilon(\varphi) = \varepsilon_0(1 + \lambda_p \cos\varphi)\sin^{-1}\gamma \tag{44}$$

Because characteristic pressure is assumed $p_0 = 4.713$ [MPa], the radial clearance has the following value [**L. 6**, **23**]:

$$\varepsilon_0 = a\sqrt{\frac{\omega\eta_0}{p_0}} = 0.001\,m\sqrt{\frac{741s^{-1}0.03Pas}{4.713MPa}} \approx 3{,}3\mu m \tag{45}$$

Numerical dimensional pressure values as the solutions of partial recurrence Equation (26) for the first UNR step performed with the Mathcad 12 and Matlab 7.2 Professional Program are depicted on the conical journal surface presented in **Fig. 8c.** The hydrodynamic pressure attains the maximum value p_{max} = 11.06 [MPa] and the load carrying capacity in y and z directions attain values C_y = 16.98N and C_z=6.18N, respectively.

For the abovementioned conical microbearing, the differences between pressure values obtained from recurrence Reynolds Equation (26) derived for the first UNR classical net and pressure values obtained from Equation (33) derived for the third UNR optimum net approximation attain about 12 percent.

CONCLUSIONS

1. This paper has presented the various geometries of the nets with calculation nods for difference methods of partial recurrence numerical solutions. The dynamic changes and conversions of particular nets occurring during the numerical calculation process have been considered. The presented theory of optimum net difference calculation is valid for various orthogonal curvilinear coordinates. Hence, the optimum net and nods geometries are considered for Reynolds equations in cylindrical, spherical, and conical coordinates and are numerically examined (see sections: 8, 9, 10).
2. As the result of the performed research, the optimum numerical net concerning the stability and convergences of the obtained numerical calculations processes for partial difference and recurrence equations have been discussed. Next, for the optimum net, the convenient Reynolds recurrence equation was derived.
3. The initial numerical calculations indicate that differences between pressure values obtained from experimental measurements and pressure values from

recurrence Reynolds Equation (26) derived for the first UNR classical net and pressure values obtained from Equation (33), derived for the third UNR optimum net approximation, attain about 7 and 3 percent, respectively. Differences between pressure values calculated by using the first and third UNR nod [**L.7**] are equal to 9 percent **Fig. 9.** [**L. 14**, **15**].

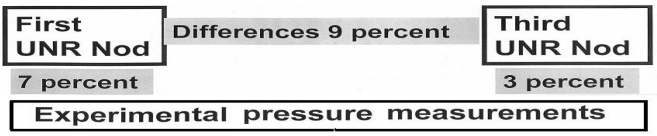

Fig. 9. Mutual differences between pressure values obtained from the first UNR nod, third UNR, Nod and Experimental measurements

Rys. 9. Wzajemne różnice między wartościami ciśnienia uzyskanymi za pomocą siatek różnicowych Pierwszego i Trzeciego Typu oraz z pomiarów doświadczalnych

REFERENCES

1. Koźniewska I.: Recurrence Equations (In Polish). PWN, Warsaw 1973.
2. Kosma Z.: Numerical Methods in Engineering Applications (in Polish), Politechnika Radomska,1999.
3. Miller K.S.: Linear difference equations, N. Y., 1968.
4. Kaczorek T.: Stability of continuous-discrete inear systems described by the general model. Bull. Pol.Ac.Tech. 59, (2), 189–192, 2011.
5. Wierzcholski K.: Unified summation equations and their applications in tribology wear process. Bulletin of the Polish Academy of Sciences Technical Sciences, vol.61, No.2, pp. 405–417, 2013.
6. Wierzcholski K.: The method of solution for hydrodynamic lubrication by synovial fluid flow in human joint gap. Control and Cybernetics, vol. 31, No.1, pp. 91–116, 2002.
7. Wierzcholski K.: Unified Mega Algorithm for Partial Recurrence Reynolds Solutions. (In English). Journal of Applied Computer Science, vol. 20, No. 1, 2012 pp. 81–101.
8. Wierzcholski K.: "Modeling and Control of Capacities in Human Joint Gap for Unsteady Periodic Motion and Magnetic Field " Journal of Applied Computer Science, vol.12, No.1, pp.127–148, 2004.
9. Wierzcholski K.: About some n-order recurrence. (In Polish). State Scientific Publishing House Pol. Acad. of Sci.(PWN), 1975.
10. Wierzcholski K.: "Solutions of Recurrence and Sum- mation Equations and Their Applications in Slide Bearing Wear Calculations". J. of Kones Powertrain and Transport, Warsaw 2012, Vol. 19, 2, pp. 543–550.
11. Kaczorek T.: Computation of positive stable realiza-tion for linear continuous-time systems, Bull. Pol.Ac.Tech. 59, (3), 273–281, 2011.
12. Demkowicz L., Gopalakrishman J.: A class of discontinuous Petrov-Galerkin methods.ii.Optimal test Functions. Num.Math.for Part.Diff.Eq. 27:70–105, 2011.

13. Center N.: Developments of a Lean,Green Automobile,Tribology and Lubrication Technology 60, pp. 15–16 (2004).
14. Kapoor A. et al.: Modern Tribology Handbook, Vol. 2, chap 32, pp. 1187–1229 Boca Raton, FL. ORC Press (2009).
15. Jang G.H., Seo C.H., Ho Scong Lee: Finite element model analysis of an HDD considering the flexibility of spinning disc-spindle", Microsystem Technologies, 13, 837–847, (2007).
16. Babuska I., Strouboulis T.: The Finite Element Method and its Reliability: Clarendon Press Oxford, 2001.
17. Babuska I., Chleboun J.: Effect of uncertainties in the domain on the solution of Dirichlet boundary value problem",Numerische Mathematik, 93, 583–610, 2003.
18. Babuska I., Oden J.T., BelytschkoT., Hughes T.J.R.: Research Directions in Computational Mechanics". Computer Methods in Applied Mechanics and Engineering",192, 913–922, 2003.
19. Babuska I., Ohnimus S.: A posteriori error estimation for the semi-discrete finite element method of parabolic differential equations", Computer Methods in Applied Mechanics and Engineering, 190:35–36, 4691–4712, 2001.
20. Ralston A.A.: First Course in Numerical Analysis (in Polish), PWN, Warsaw 1971.
21. Levy H., Lessman F.: Finite Recurrence Equations (In Polish), PWN, Warsaw 1966.
22. Kiełbasiński A., Schwetlick K.: Linear numerical algebra (In Polish), WNT, Warsaw 1994.
23. Wierzcholski K.: Bio and Slide Bearings:Their Lubrication By Non-Newtonian Fluids and Applications in Non-Conventional Systems. Vol. III, Gdańsk University of Technology, 2007.

Streszczenie

Współczesne problemy obliczeń numerycznych występujące w tribologicznych problemach urządzeń napędowych oraz w problemach sprzętu transportowego a szczególnie w mikrołożyskach ślizgowych twardych dysków komputerowych wymagają uzyskiwania coraz to większych dokładności wraz z zachowaniem własności inteligentnych. Ponadto w przeprowadzanych obliczeniach istotną rolę odgrywa zbieżność, stabilność, a także niezawodność uzyskanych wartości numerycznych. Główny temat naukowy przedstawionego artykułu koncentruje się na metodzie identyfikowania optymalnej siatki różnicowej do numerycznych rozwiązań cząstkowych równań rekurencyjnych i różnicowych.

Dlatego też została przeprowadzona optymalizacja geometrycznej lokalizacji węzłów obliczeniowych oraz ich dynamika zmian w trakcie obliczeń numerycznych. Wyprowadzony oraz zdefiniowany został indeks optymalizacji określający najbardziej korzystną geometrię lokalizacji węzłów obliczeniowych w trakcie przeprowadzanych obliczeń numerycznych.

Optymalnie dobrana siatka obliczeń w metodach różnicowo-rekurencyjnych ma związek ze stabilnością uzyskiwanych rozwiązań numerycznych oraz zapewnia zbieżność procesu obliczeniowego dla różnych krzywoliniowych geometrii ortogonalnych. Zdefiniowana została tak zwana Jednostkowa Siatka Obszaru (UNR) dla różnych czterech typów aproksymacji różnicowej. Dla dwóch wybranych typów aproksymacji numerycznej opracowano schematy różnicowe, a następnie na ich podstawie przy wykorzystaniu Programu Mathcad 12 wyznaczono wartości ciśnienia i siły nośnej ze zmodyfikowanego równania Reynoldsa w przypadku trzech najczęściej występujących czopów w mikrołożyskach ślizgowych HDD, a mianowicie walcowych, parabolicznych oraz stożkowych.

Porównane zostały odchylenia w zakresie uzyskanych wartości ciśnienia hydrodynamicznego wyznaczonych przy wykorzystaniu dwóch różnych procesów aproksymacji różnicowej. Mianowicie porównano wyniki uzyskane dla pierwszego klasycznego najczęściej spotykanego typu aproksymacji z wartościami wyznaczonymi z trzeciego bardziej zaawansowanego typu aproksymacji różnicowej. Wartości te mogą różnić się od kilku do dziesięciu procent. Następnie wyprowadzone zostały wnioski dotyczące tworzenia optymalnych lokalizacji geometrii węzłów dla innych operatorów różnicowych rekurencyjnych w przestrzeniach dyskretnych.